Inventory of Supplementary Materials

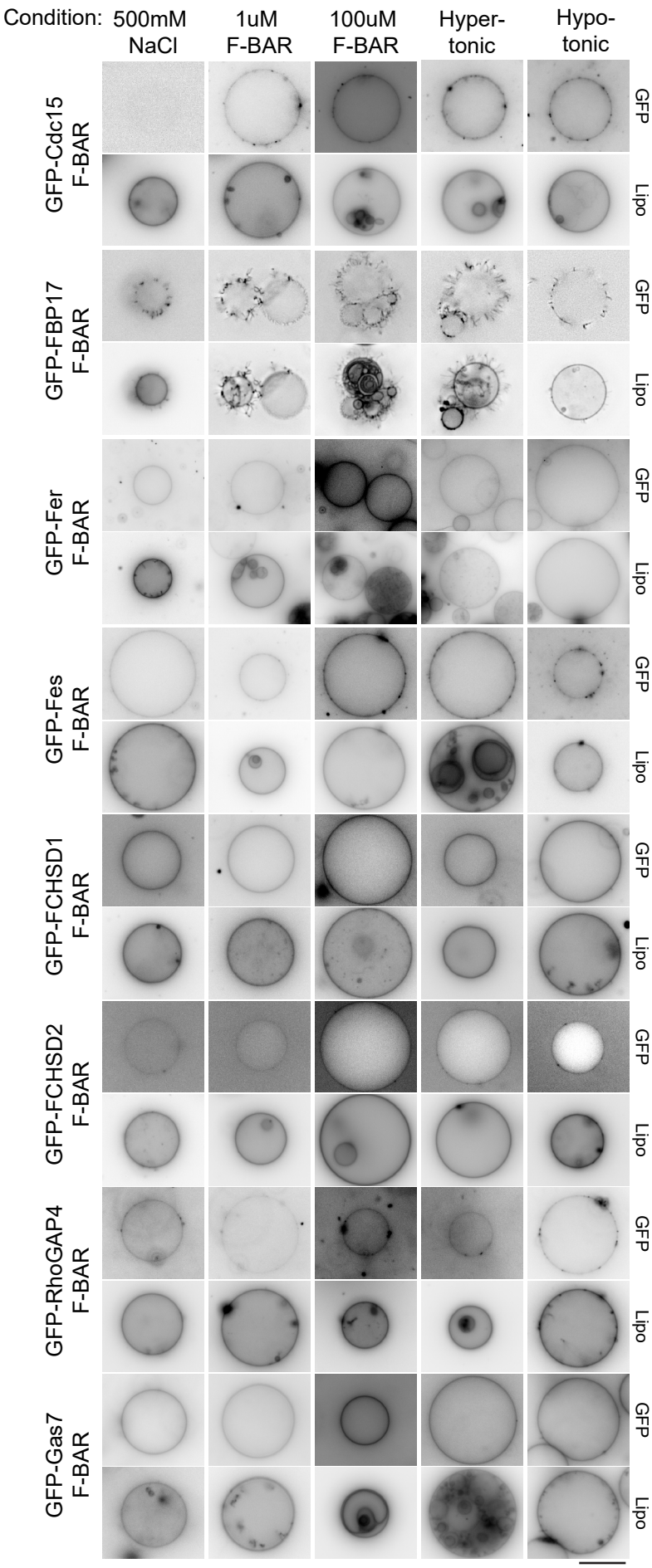

McDonald et al. Figure S1

Figure S1, related to Figure 3. Cdc15 and 6 human F-BARs do not tubulate membranes under a variety of conditions. The indicated F-BAR domains were mixed with GUVs (composed of 69% DOPC / 15% DOPE / 10% DOPS / 5% PI(4)P / 1% Rhodamine-PE) in the indicated buffer condition. Concentrations of F-BARs were 10 µM and NaCl 150 mM unless otherwise indicated. Scale bar = 10 µm.

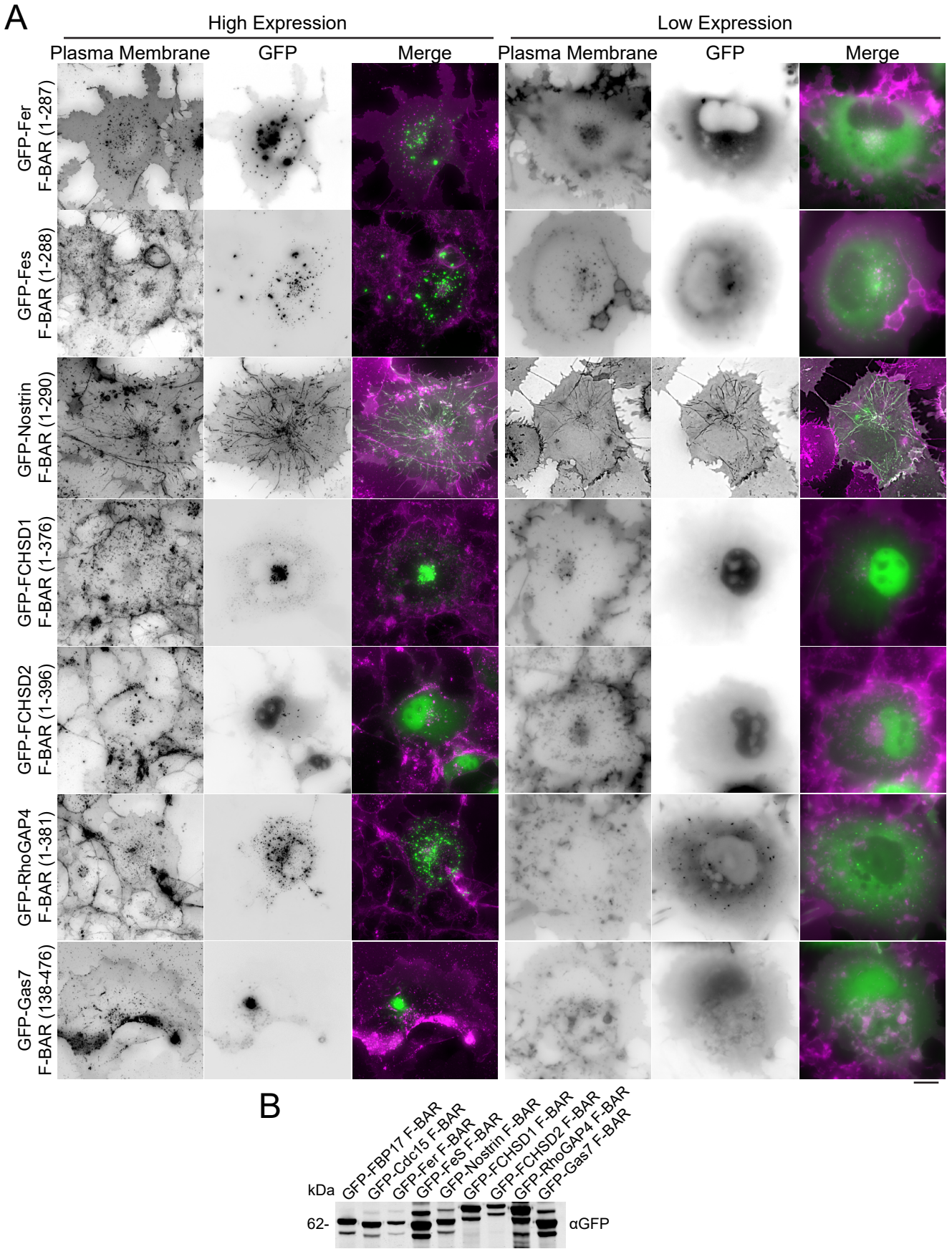

McDonald et al, Figure S2

Figure S2, related to Figure 3. A significant fraction of human F-BAR domains do not tubulate membranes in vivo. A) Expression of the indicated GFP-F-BAR domains in COS-7 mammalian cells, co-stained with CellMask Orange plasma membrane stain. High and low expression example cells for each condition are shown. Scale bar = 10 µm. B) Anti-GFP immunoblot showing expression of GFP-F-BAR domain constructs in COS-7 cell lysates.

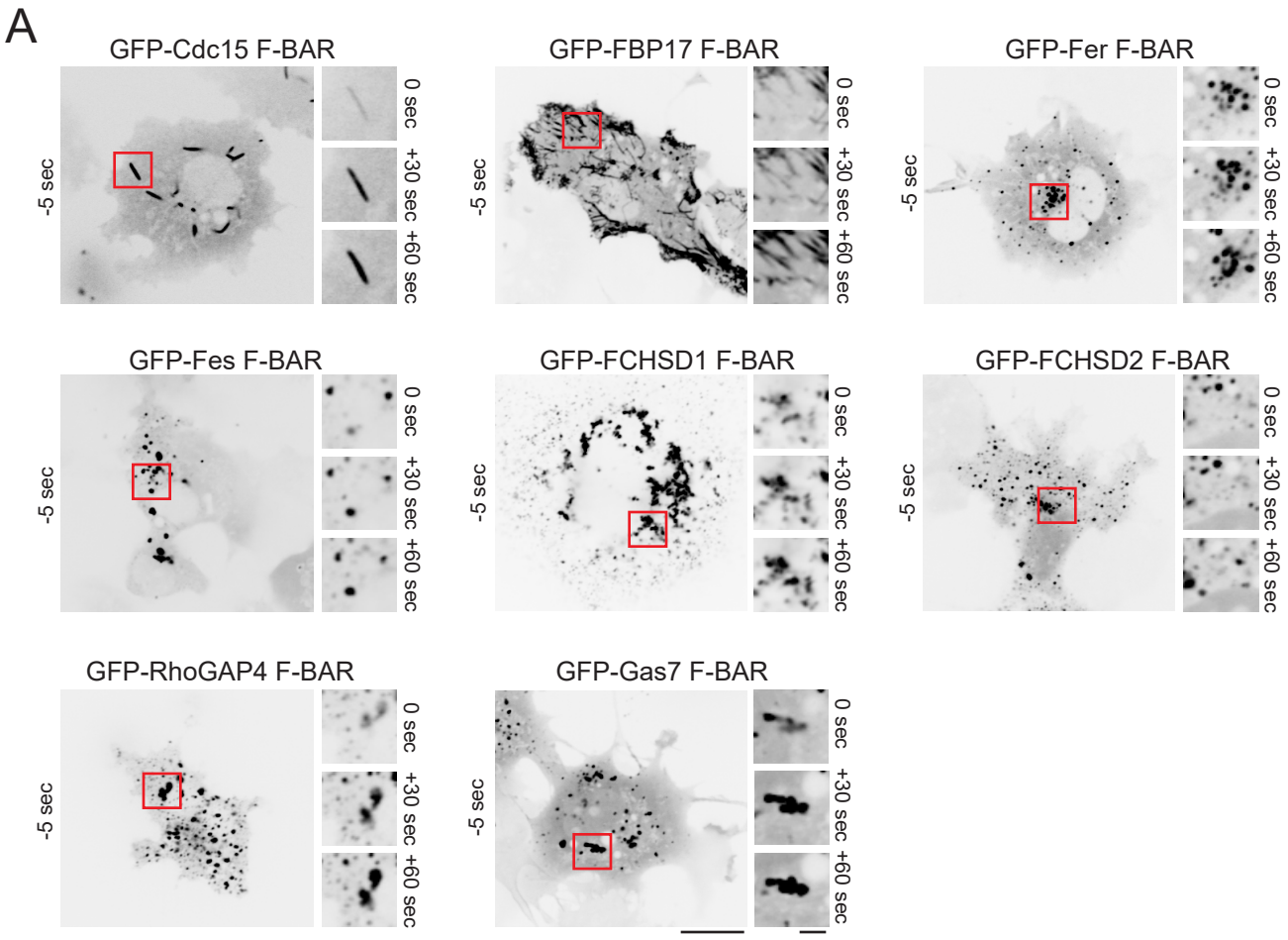

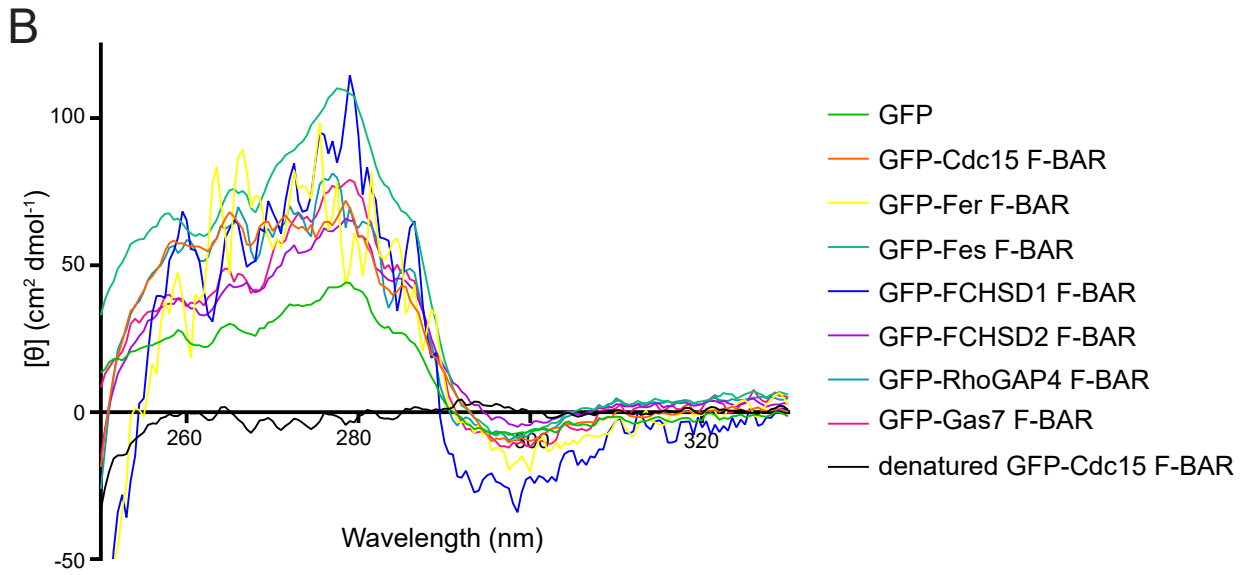

McDonald et al, Figure S3

Figure S3, related to Figure 3. Cdc15 and other F-BAR domains are folded and functional.

A) FRAP assay of the indicated transfected construct in COS-7 cells. The area in each red square was bleached. Scale bars = 10 µm (main image) and 2 µm (inset). B) Near-UV circular dichroism spectra of GFP and each GFP-F-BAR domain.

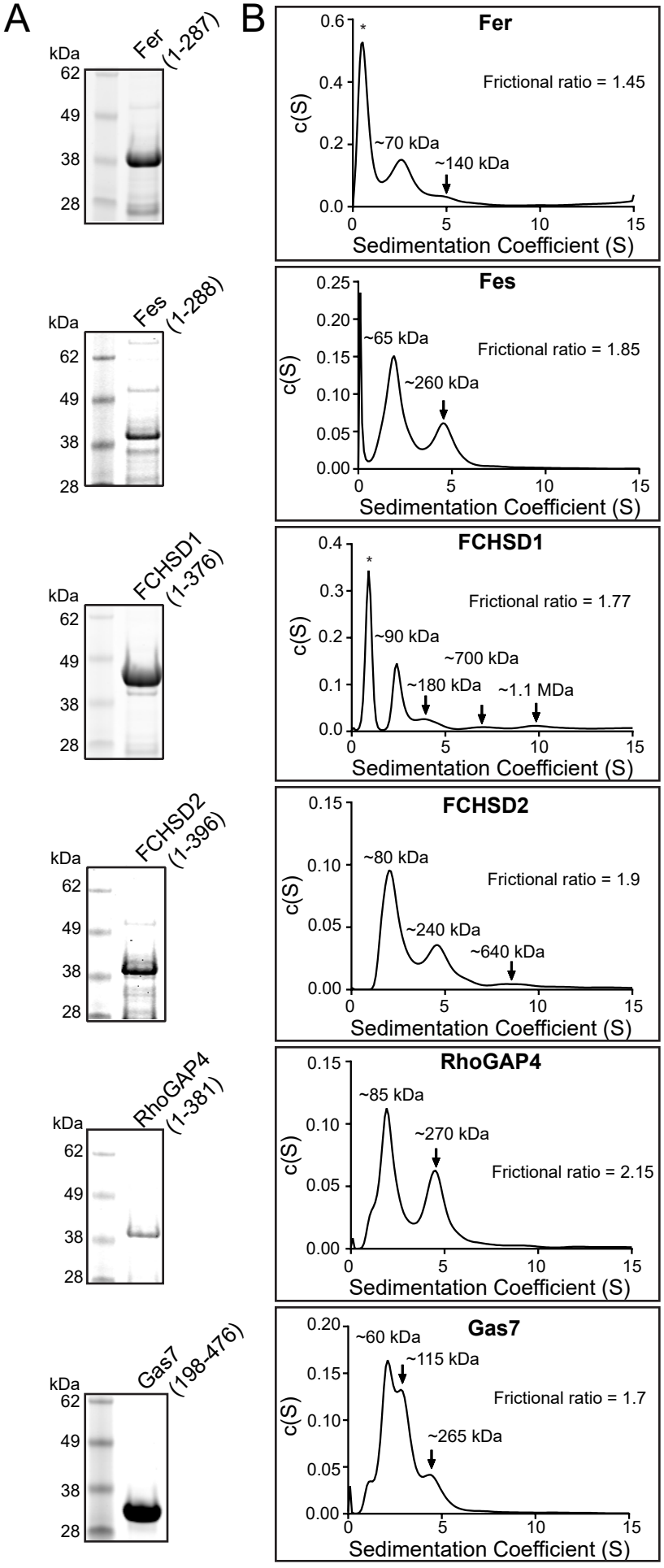

McDonald et al, Figure S4

Figure S4, related to Figure 4. Non-tubulating human F-BAR domains show evidence for oligomerization in solution. A) Coomassie stained SDS-PAGE of the indicated purified F-BARs. B) Analytical ultracentrifugation traces of the indicated human F-BAR domains. Arrows indicate oligomerized species. * indicates small MW contaminates.

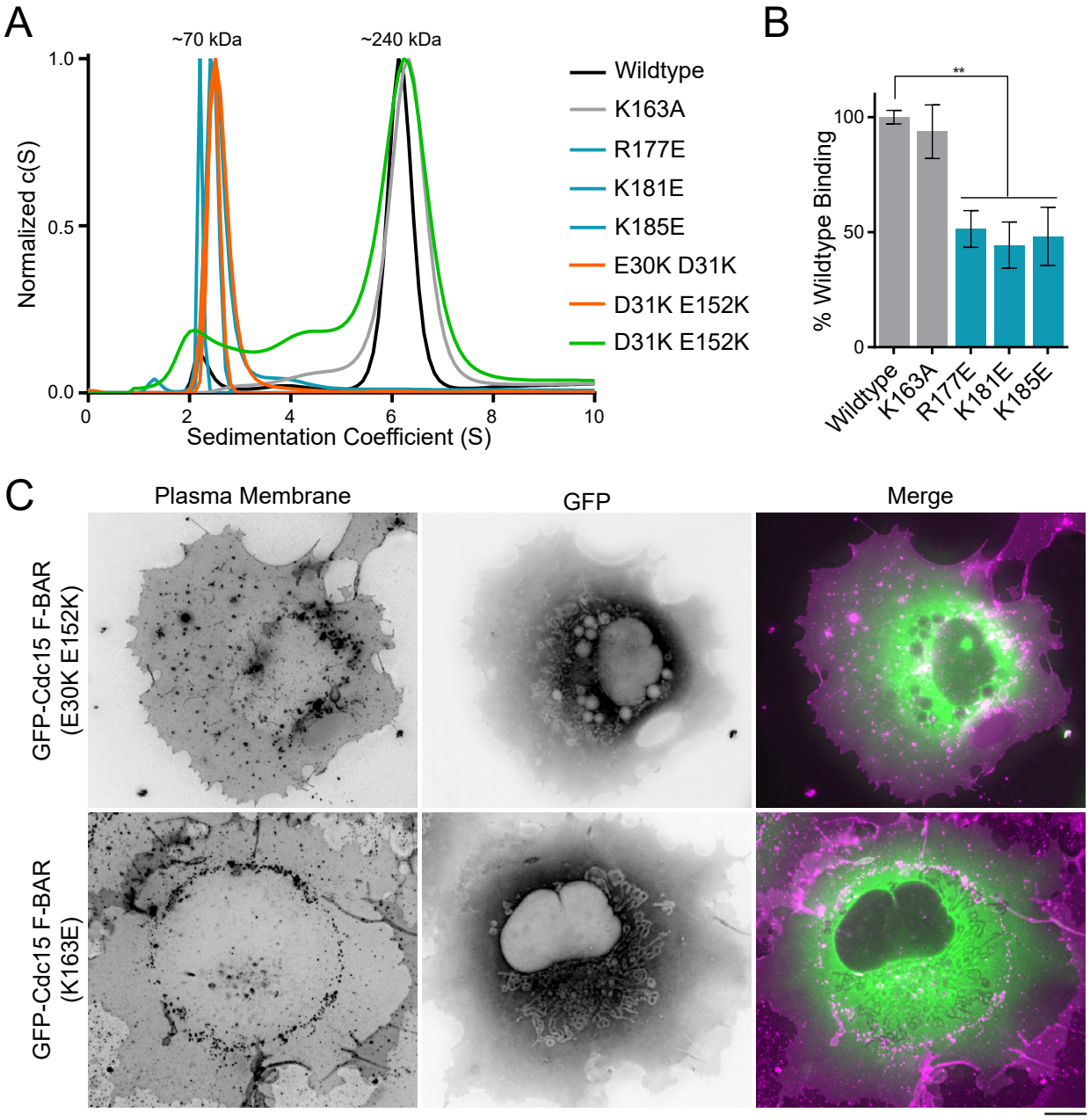

McDonald et al, Figure S5

Figure S5, related to Figure 5. F-BAR domain oligomerization and membrane binding. A) Analytical ultracentrifugation traces of additional Cdc15 F-BAR domain mutants. B) Bio-Layer Interferometry binding assay between additional Cdc15 F-BAR domain mutants at 1 μM and 100 nm liposomes composed of 69.9% DOPC / 15% DOPE / 10% DOPS / 5% PI(4)P / 0.1% Biotin-PE. Error bars indicate SEM. **, $p<0.01$, one-way ANOVA. C) GFP-Cdc15 F-BAR domain mutants were expressed in COS-7 cells and co-stained with CellMask Orange plasma membrane dye. Scale bar = 10 μm.

A

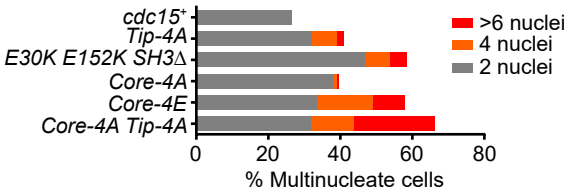

B

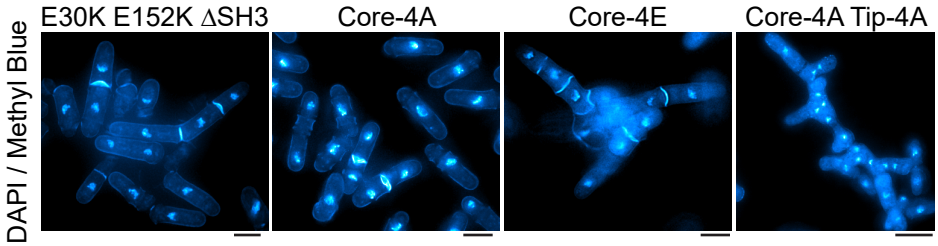

C

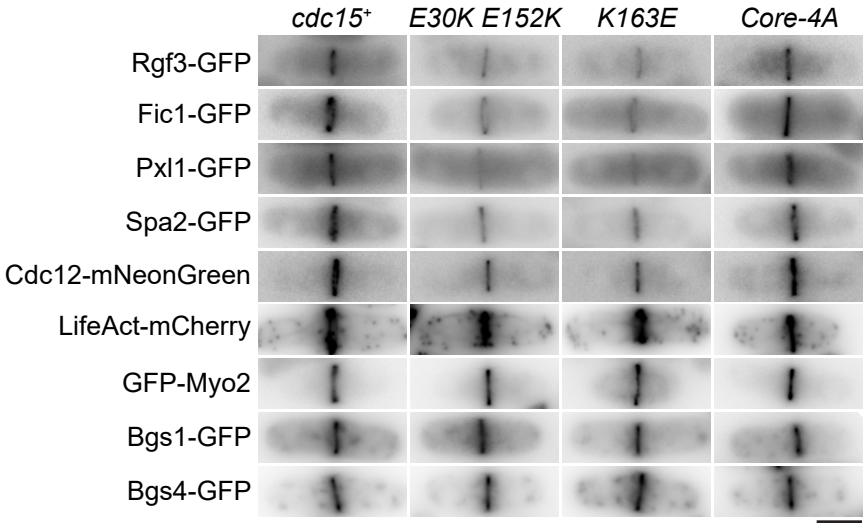

D

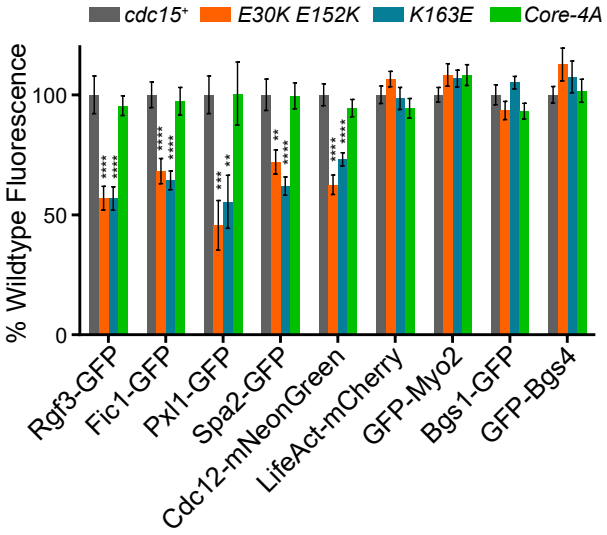

E

cdc15(E30K E152K)			
myo2-E1	lethal	*cdc12-112*	sick
cdc4-8	lethal	*cps1-191*	sick
imp2Δ	lethal	*fic1Δ*	sick
rng2-D5	lethal	*mid1Δ*	none
pxl1Δ	lethal	*rgf3-s44*	none
sid2-250	lethal	*spa2Δ*	none

McDonald et al, Figure S6

Figure S6, related to Figure 6. Oligomerization is critical for Cdc15 function in cytokinesis. A) Number of nuclei per cell in the indicated *cdc15* mutants. Wildtype data is from Figure 7B. n > 400 for each genotype. B) DAPI (DNA) and Methyl Blue (cell wall / septum) staining of the indicated *cdc15* mutants. C-D) Representative sum projection images (C) and quantification (D) of contractile ring fluorescence intensity of the indicated fluorescently tagged proteins in *cdc15*$^{+}$*, cdc15(E30K E152K)*, *cdc15(K163E)*, or *cdc15(Core-4A)* strains. n>50 for each condition. Error bars indicate SEM. **, p<0.01; ***, p<.001; ****, p<.0001, one-way ANOVA. E) Summary of *cdc15(E30K E152K)* synthetic genetic interactions. See also Figure S7. All scale bars = 4 µm.

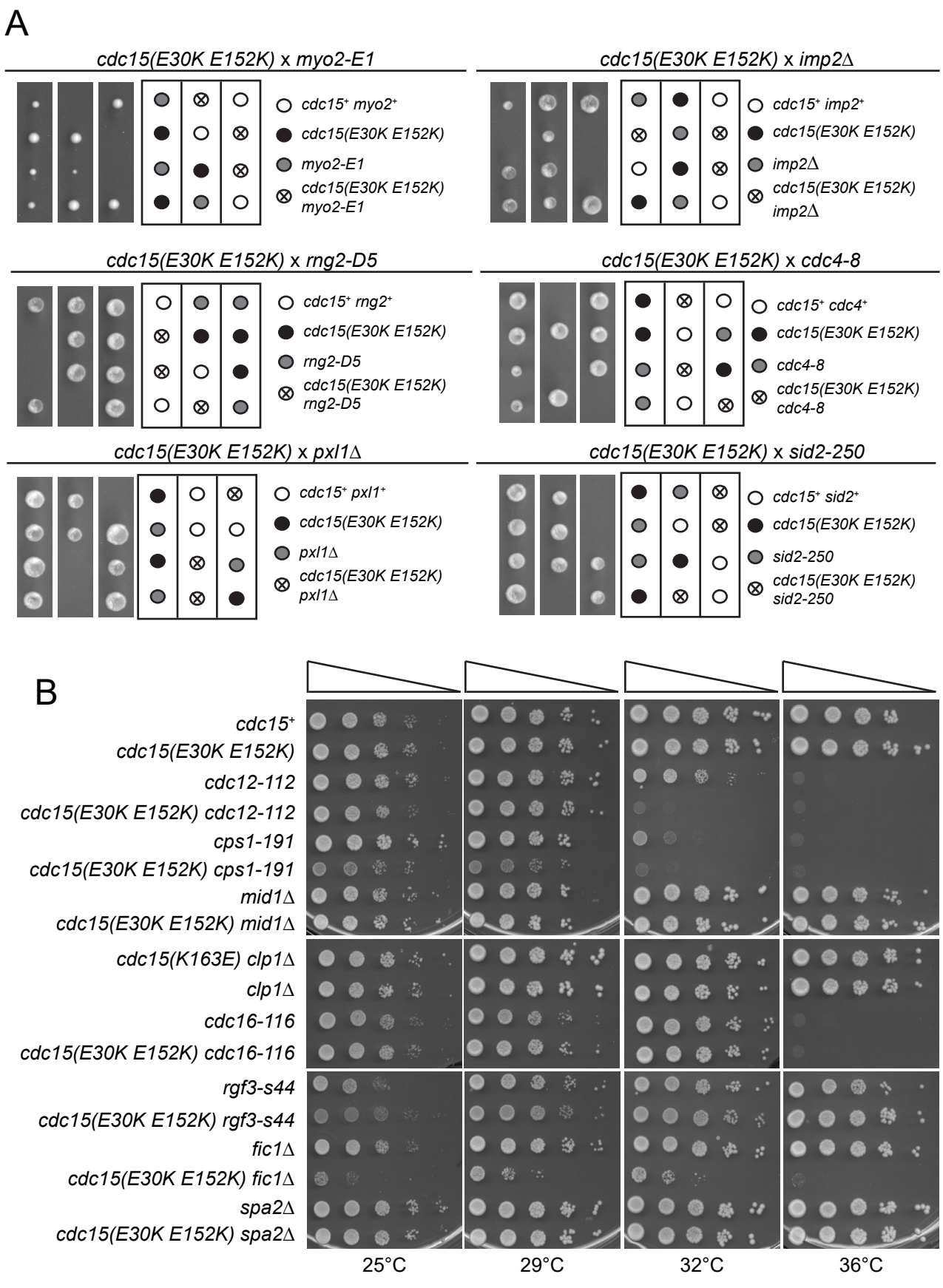

McDonald et al, Figure S7

Figure S7, related to Figure 6. Cdc15 oligomerization mutant genetic interactions. A) Representative tetrad dissections from the indicated *cdc15(E30K E152K)* crosses. Relevant genotypes are indicated. B) Serial dilutions of indicated strains grown at different temperatures.

Table S1, related to Figure 3. Membrane tubulation by human F-BAR domains.

Gene	Protein	Tubulation (+/-/none)*	First reported (in vivo, in vitro)
CIP4	Cdc42-interacting protein 4	+	in vivo, in vitro (Tsujita et al., 2006)
FBP17	Formin-binding protein 17	+	in vivo (Kamioka et al., 2004) in vitro (Tsujita et al., 2006)
FCHO1	FCH domain only protein 1	+	in vivo, in vitro (Henne et al., 2010)
FCHO2	FCH domain only protein 2	+	in vitro (Henne et al., 2007) in vivo (Henne et al., 2010)
FCHSD1	FCH and double SH3 domain protein 1	none	in vivo, in vitro (this study)
FCHSD2	FCH and double SH3 domain protein 2	none	in vivo, in vitro (this study)
FER	Tyrosine protein kinase	none	in vivo (Tsujita et al., 2006) in vitro (this study)
FES	Tyrosine protein kinase	none	in vivo, in vitro (this study)
GAS7	Growth arrest specific protein 7	none	in vivo, in vitro (this study)
NOSTRIN	Nitric oxide synthase trafficking	+	in vivo, in vitro (this study)
PACSIN1	Protein kinase C and casein kinase substrate in neurons protein 1	+	in vitro (Wang et al., 2009)
PACSIN2	Protein kinase C and casein kinase substrate in neurons protein 2	+	in vivo (Shimada et al., 2010) in vitro (Bai et al., 2012)
PACSIN3	Protein kinase C and casein kinase substrate in neurons protein 3	+	in vitro (Bai et al., 2012)
PSTPIP1	Proline-serine-threonine phosphatase interacting protein 1	+	in vivo, in vitro (Tsujita et al., 2006)
PSTPIP2	Proline-serine-threonine phosphatase interacting protein 2	+	in vivo (Tsujita et al., 2006)
RHOGAP4	Rho GTPase activating protein 4	none	in vivo, in vitro (this study)
SRGAP1	SLIT-ROBO Rho GTPase-activating protein 1	-	in vivo (Coutinho-Budd et al., 2012)
SRGAP2A/ B/C	SLIT-ROBO Rho GTPase-activating protein 2A/B/C	-	in vivo, in vitro (Guerrier et al., 2009)
SRGAP3	SLIT-ROBO Rho GTPase-activating protein 3	-	in vivo (Carlson et al., 2011)
TOCA1	Transducer of Cdc42-dependent actin assembly	+	in vivo (Kakimoto et al., 2006) in vitro (Wang et al., 2009)

*+, positive membrane curvature; -, negative membrane curvature.

Movie S1, related to Figure 6. Time-lapse of *cdc15(E30K E152K)-mCherry sid4-GFP* cells failing cytokinesis. Time overlay indicates minutes from spindle pole body separation.

Movie S2, related to Figure 6. Time-lapse of *cdc15(K163E)-mCherry sid4-GFP* cells failing cytokinesis. Time overlay indicates minutes from spindle pole body separation.

Supplemental Experimental Procedures

Yeast Strains, Media, and Genetics

S. pombe strains (see "*S. pombe strains used in this study"* below) were grown in yeast extract (YE) media or 4X YE for large scale purifications. *cdc15* mutants were integrated at the endogenous locus by rescuing cdc15^{+}/*cdc15::ura4*$^{+}$ diploids with *pIRT2-cdc15* mutant constructs containing 5' and 3' noncoding flanks. Haploid integrants resistant to 5-fluorourotic acid (5-FOA) were isolated and the *cdc15* mutations were verified by PCR and sequencing. *cdc15* diploids for tetrad dissection assays were created by integrating constructs containing 5' and 3' noncoding flanks and a kan^{R} marker 3' to the cdc15 gene in a *cdc15+/cdc15::ura4*$^{+}$ diploid strain. Integrants resistant to 5-FOA and G418 were selected and verified before sporulation and tetrad dissection. *cdc15* and *cdc15* mutants were tagged endogenously at their 3' termini with kan^{R}, hygr^{R}, mCherry- kan^{R}, EGFP- kan^{R}, or TEV-2xProtA- kan^{R} (Bähler et al., 1998). Transformations of *S. pombe* cells were performed with a lithium acetate method (Keeney and Boeke, 1994). Standard methods were used for genetic crosses and tetrad analyses.

Cell Culture

COS-7 cells were grown in DMEM media + 10% FBS (Life Technologies). COS-7 cells were plated for transfection and microscopy on glass slides or MatTek glass bottom dishes (MatTek Corporation, Ashland, MA) coated with fibronectin (Sigma-Aldrich). When assaying tubulation (Figures 2, S2, and S3) pEGFP F-BAR constructs were transfected into COS-7 cells with Lipofectamine 3000 reagents according to manufacturer's protocols for 24 hours (Life Technologies), co-stained with CellMask Orange plasma membrane dye for 5 minutes at 37°C (Life Technologies), and immediately imaged. pEGFP Fer constructs (Figure 7) were also transfected with Lipofectamine 3000 reagents, but COS-7 cells were fixed after 24 hours with 4% paraformaldehyde, permeabilized with 0.2% NP-40, and co-stained with Rhodamine-

phalloidin before imaging (Cytoskeleton, Denver, CO) (Itoh et al., 2009). A COS-7 wound healing assay was performed as previously described for RhoGAP4 (Vogt et al., 2007). ~80-90% confluent COS-7 cells were transfected with pEGFP RhoGAP4 constructs for 24 hours before a wound was created with a P200 pipet tip. Expression of transfected F-BARs was confirmed by lysing cells in ice-cold RIPA buffer for 30 minutes, SDS-PAGE, and anti-GFP (Roche) immunoblotting.

Molecular Biology

Cdc15 constructs were created by amplifying Cdc15 fragments (19-312) by PCR from pKLG4456 and subsequent cloning into pREP81 for regulated expression in *S. pombe*, pIRT2 for integration at the endogenous locus (Roberts-Galbraith et al., 2009), pET15b for expression in bacteria, or pEGFP-C1 for expression in COS-7 cells. Human F-BAR constructs were made by amplifying F-BAR sequences from Mammalian Gene Collection clones (GE Dharmacon) and subsequent cloning into pEGFP-C1 or pET15b. GFP-F-BAR constructs were created by subcloning GFP with an 11 residue C-terminal linker (-GGGGSGGGGSG-) into NdeI sites in pET15b F-BAR constructs. Cdc15 F-BAR mutations were made in pET15b, pEGFP, and pIRT2 constructs with a QuikChange Site-Directed Mutagenesis kit (Agilent Technologies). All constructs were sequenced for verification.

Protein Purification

F-BARs and GFP-F-BARs were produced in *Escherichia coli* Rosetta2(DE3)pLysS cells grown in TB by inducing expression in log phase with 0.4 mM IPTG overnight at 18°C. His-tagged proteins were purified on cOmplete His-Tag resin (Roche) in 50mM Tris pH 8.0, 300mM NaCl, 5 mM β-mercaptoethanol. His tags were removed by thrombin digestion (recothrom at 1:100) for 2 hours at room temperature and F-BARs were further purified on a HiTrap Q SP anion exchange column (GE Healthcare) or a HiPrep Sephacryl S-100HR gel filtration column (GE Healthcare)

before being concentrated to ~1-5 mg/mL with Amicon Ultra Centrifugal Filters (Millipore). Full length Cdc15-TEV-2xProtA was purified from *S. pombe* pellets (from 2L of 4X YE) on IgG Sepharose fast flow 6 resin (GE Healthcare) in NP-40 buffer with protease inhibitors (10 mM sodium phosphate pH 8.0, 150 mM NaCl, 1% NP-40, 2mM EDTA, 1mM PMSF, 2mM Benzamidine, 5mM DIFP, and protease inhibitor tablets (Roche)), with additional 1 M NaCl NP-40 buffer washes to eliminate co-purification of binding partners. Full length proteins were cleaved off IgG beads with TEV protease for 2 hours at 16°C and concentrated with Amicon Ultra Centrifugal Filters (Millipore). Cleavage samples were blotted with an αCdc15 polyclonal antibody(Roberts-Galbraith et al., 2009).

Liposome Binding

All lipids were obtained from Avanti Polar Lipids. Liposomes were formed as previously described (Itoh et al., 2005). Briefly, $CHCl_3$ lipid stocks were mixed at the desired ratios and evaporated in a glass tube under N_2 stream, vacuum dried for 1 hour, rehydrated in 20 mM HEPES pH 7.4, 150 mM NaCl buffer before vortexing, 10 cycles of freeze-thawing, and extrusion to various sizes with an Avanti mini-extruder. Liposome co-pelleting assays were performed as previously described (Itoh et al., 2005), where 100 uL of 1 mg/mL liposomes were mixed with 100 uL of Cdc15 F-BAR (10-20 µg total) for 15 min at room temperature before centrifugation at 150,000 xg in an Optima TL ultracentrifuge for 15 min at 25˚C. Supernatant and pellet fractions were separated and run on SDS-PAGE. Giant Unilamellar Vesicles (GUVs) were formed by drying 10 µL of 10 mg/mL $CHCl_3$ lipids (69% DOPC, 15% DOPE, 10% DOPS, 5% PI(4)P, 1% Rhodamine-PE) on Indium-Tin-Oxide-coated (ITO) glass coverslips (Sigma-Aldrich) under N_2 stream followed by vacuum for 1 hour. A 2 mm chamber was assembled between the coverslips and filled with a 20 mM HEPES pH 7.4 and 500 mM sucrose buffer through which a 10 Hz, 2.5 V sinusoidal current was passed for 2 hours. After formation, NaCl was added to 150 mM final concentration. For hypo- and hyper-tonic buffer condition

experiments, equal volumes of 20 mM HEPES pH 7.4, 150 mM NaCl or 20 mM HEPES pH 7.4, 150 mM NaCl +100 mM sucrose, respectively, was added to the GUVs before F-BAR addition. Recombinant GFP-F-BAR domain solutions were mixed with GUVs at a final concentration of 10 µM (unless otherwise indicated) before imaging in a 0.5 mm chamber. Liposome binding experiments were performed through Bio-Layer Interferometry on an Octet RED96 instrument (ForteBio, Menlo Park, CA) using streptavidin sensor tips (Abdiche et al., 2008). A standard association experiment was performed: streptavidin tips were equilibrated in buffer (20 mM HEPES pH 7.4, 200 mM NaCl) for 120s, blocked with 10 mg/mL BSA for 180s, 100 nm liposomes (containing 0.1% Biotin-PE and the various compositions indicated in the text) were bound for 300s, tips were washed 2x for 180s, and 1 µM F-BAR association to equilibrium was monitored for 300s. Raw data was normalized for unequal liposome loading and nonspecific binding was subtracted from a control sensor tip without liposomes; equilibrium binding levels were calculated across at least 3 experiments. One-way ANOVA tests were used to determine significance values between binding conditions and mutants.

Microscopy

S. pombe cells were imaged live at 25°C or fixed with ice-cold 70% ethanol and stained with Methyl Blue and DAPI before imaging. GUV, *S. pombe,* and COS-7 cell imaging was performed on a Personal DeltaVision microscope system (Applied Precision) that includes an Olympus IX71 microscope, a 60X NA 1.42 planApo objective, and a Photometrics Coolsnap HQ2 camera. Time-lapse imaging was performed on log-phase cells using an ONIX microfluidics perfusion system, flowing YE media at 25°C through the chamber at 5 psi throughout imaging. Image stacks were deconvolved using softWoRx imaging software. Cdc15 FRAP experiments were performed on a Zeiss LSM510 META microscope system with a 63X plan-Apochromat objective. COS-7 cell FRAP experiments were performed on a spinning disk system which includes a Zeiss Axiovert200m microscope, Yokogawa CSU-22, 63X NA 1.46 planApochromat

objective, Hamamatsu ImageEM-X2 camera, and an Andor Micropoint bleaching system. COS-7 wound healing images were acquired on an EVOS FL imaging system (ThermoFisher) with a 10X objective. Image projections, intensity measurements, and FRAP analyses were performed with ImageJ software (http://rsweb.nih.gov/ij/). Lamellipodia were considered arc-shaped membrane edges with decreasing actin staining intensity with increasing distance toward the cell middle (Itoh et al., 2009). Quantification of COS-7 wound healing was performed by measuring the advancement of the leading cell edge into the wound after 8 hours as a percentage of the original wound area. One-way ANOVA tests were used to determine significance values between conditions.

Electron Microscopy

5 uL of 1 ug/mL Cdc15 F-BAR solution diluted into 50 mM NaCl, 20 mM Tris-HCl pH 7.4 for oligomer visualization alone (Figure 4C), or 5 uL of 1:1 1mg/mL liposomes (composed of 70% DOPC / 15% DOPE / 10% DOPS / 5% PI(4)P):10uM final concentration F-BARs in 150mM NaCl, 20 mM Tris-HCl pH 7.4 for liposome bound samples (Figures 2B and 3B), was adsorbed to a glow discharged 200-mesh copper grid covered with carbon-coated collodion film (EMS, Hatfield, PA). For oligomer bound samples in Figure S4, 1 mg/mL Cdc15 F-BAR was mixed with 1 mg/mL liposomes at 200 mM NaCl to allow membrane binding. This sample was diluted to 100 mM NaCl to induce oligomerization before 5 uL was added to an EM grid. Grids were washed in two drops of water to remove unbound sample and stained with two drops of 0.75% uranyl formate (Ohi et al., 2004). Samples were imaged on a FEI Morgagni electron microscope operated at 100 kV and images were captured at 18,000-36,000X on a 1K x 1K CCD camera (ATM, Woburn, MA).

Analytical Ultracentrifugation

F-BAR domains were diluted to a final concentration of 0.5 mg/mL and 50 mM NaCl to induce oligomerization before ultracentrifugation. Sedimentation experiments were run at 42,000 rpm at 4°C on an Optima XLI ultracentrifuge (Beckman-Coulter) with a four-hole An60Ti rotor. 1.2 cm path-length centerpieces with sapphire windows were used to collect 280 and 230 nm scan data. Velocity scans were analyzed with SedFit (version 14.81) using 250 scans collected ~2 min apart (Schuck, 2000). Size distributions were determined for a confidence level of $p = 0.95$ and resolution of $n = 200$.

Circular dichroism

Circular dichroism measurements were performed on a Jasco J-810 spectropolarimeter between 330-250nm. Scans were acquired at 20nm/min with 4 sec response times, a 1 nm bandwidth, and 4 accumulations. Ellipticity measurements were converted to molar ellipticity for presentation [θ] (cm^2dmol^{-1}).

Structural Modelling

The Cdc15 F-BAR domain structural model was generated using the Protein Homology/analogY Recognition Engine V 2.0 (Phyre^2) (Kelley and Sternberg, 2009) with the Hof1 F-BAR as a template structure (PDB 4WPE) using the one-to-one threading mode. Fer and RhoGAP4 F-BAR domain models were generated in the standard mode, which identified Fes (PDB: 4DYL) and CIP4 (PDB: 2EFK) F-BAR structures as homologous templates, respectively. Negatively charged surface patches along the sides of the Fer and RhoGAP4 F-BAR models were identified with the use of surface electrostatic potential maps. Mutations tested for inhibition of oligomerization included: Fer – 1) E90K, D91K, E239K 2) E124K, E132K 3) E265K and 4) E276K, E278K, D280K; RhoGAP4 – 1) E122K 2) E155K, E156K, E159K 3) E182K, E187K, E192K 4) D304K, D307K. Graphical representations of the F-BAR model were generated using PyMOL (Schrodinger, LLC).

S. pombe strains used in this study

Strain	Genotype	Source
Figure 1		
KLG18191	*cdc15^{+} / cdc15 F-BAR(1-319):KanR ade6-m210 / ade6-m216 leu1-32 / leu1-32 ura4-D18 / ura4-D18 diploid*	this study
KLG18192	*cdc15^{+} / cdc15(327-927):KanR ade6-m210 / ade6-m216 leu1-32 / leu1-32 ura4-D18 / ura4-D18 diploid*	this study
Figure 5		
KLG7476	*cdc15-TEV-2xProtA:Kan^{R} ade6-M21X leu1-32 ura4-D18 h^{-}*	(Roberts-Galbraith et al., 2010)
KLG17817	*cdc15(E30K E152K)-TEV-2xProtA:Kan^{R} ade6-M21X leu1-32 ura4-D18 h^{-}*	this study
KLG16373	*cdc15(K163E)-TEV-2xProtA:Kan^{R} ade6-M21X leu1-32 ura4-D18 h^{-}*	this study
Figure 6		
KLG17863	*cdc15^{+} / cdc15(Core-4E K163E):Kan^{R} ade6-M210 / ade6-M216 ura4-D18 / ura4-D18 leu1-32 / leu1-32 diploid*	this study
KLG7326	*cdc15-mCherry:Kan^{R} ade6-M210 leu1-32 ura4-D18 h^{-}*	lab stock
KLG17101	*cdc15(E30K E152K)-mCherry:Kan^{R} ade6-M21X leu1-32 ura4-D18 h^{-}*	this study
KLG16187	*cdc15(K163E)-mCherry:Kan^{R} ade6-M21X leu1-32 ura4-D18 h^{-}*	this study
KLG17748	*cdc15(Core-4A)-mCherry:Kan^{R} ade6-M21X leu1-32 ura4-D18 h^{-}*	this study
KLG3019	*cdc15-GFP:Kan^{R} ade6-M210 leu1-32 ura4-D18 h^{-}*	lab stock
KLG17100	*cdc15(E30K E152K)-GFP:Kan^{R} ade6-M21X leu1-32 ura4-D18 h^{-}*	this study
KLG17400	*cdc15(K163E)-GFP:Kan^{R} ade6-M21X leu1-32 ura4-D18 h^{-}*	this study
KLG17747	*cdc15(Core-4A)-GFP:Kan^{R} ade6-M21X leu1-32 ura4-D18 h^{-}*	this study
KLG246	*ade6-m210 leu1-32 ura4-D18 h^{-}*	lab stock
KLG17094	*cdc15(E30K E152K) ade6-M21X leu1-32 ura4-D18 h^{-}*	this study
KLG16009	*cdc15(K163E) ade6-M21X leu1-32 ura4-D18 h^{-}*	this study
KLG7450	*rlc1-GFP:ura4^{+} sid4-GFP:Kan^{R} ade6-M21X leu1-32 ura4-D18 h^{-}*	lab stock
KLG17104	*cdc15(E30K E152K):Kan^{R} rlc1-GFP:ura4^{+} sid4-GFP:Kan^{R} ade6-M21X leu1-32 ura4-D18 h^{-}*	this study
KLG17409	*cdc15(K163E):Kan^{R} rlc1-GFP:ura4^{+} sid4-GFP:Kan^{R} ade6-M21X leu1-32 ura4-D18 h^{-}*	this study
KLG17891	*cdc15(E30K E152K)-mCherry:Kan^{R} sid4-GFP:Kan^{R} ade6-M21X leu1-32 ura4-D18 h^{-}*	this study
Figure S7		
KLG4407	*rgf3-GFP:Kan^{R} ade6-M210 leu1-32 ura4-D18 h^{-}*	lab stock
KLG6522	*fic1-GFP:Kan^{R} ade6-M210 leu1-32 ura4-D18 h^{-}*	lab stock
KLG16699	*pxl1-GFP:Kan^{R} ade6-M210 leu1-32 ura4-D18 h^{+}*	lab stock
KLG7420	*spa2-GFP:Kan^{R} ade6-M210 leu1-32 ura4-D18 h^{+}*	lab stock
KLG16752	*cdc12-mNeonGreen:Kan^{R} ade6-M21X leu1-32 ura4-D18 h^{-}*	(Willet et al., 2015)
KLG14569	*pAct1-LifeAct-mCherry::leu1^{+} ade6-M216 leu1-32 ura4-D18 h^{-}*	(Huang et al., 2012)
KLG5298	*GFP-myo2:Kan^{R} ade6-M210 leu1-32 ura4-D18 h^{+}*	(Wu and Pollard, 2005)

KLG3512	*bgs1-GFP:KanR leu1-32 ura4-D18 h$^-$*	Mohan Balasubramanian
KLG11110	*GFP-bgs4::leu1$^+$ bgs4::ura4$^+$ leu1-32 ura4-D18 his3D-1*	(Cortés et al., 2005)
KLG17851	*cdc15(E30K E152K) fic1-GFP:Kan^R ade6-M21X leu1-32 ura4-D18 h$^-$*	this study
KLG17853	*cdc15(E30K E152K) pxl1-GFP:Kan^R ade6-M21X leu1-32 ura4-D18 h$^-$*	this study
KLG17854	*cdc15(E30K E152K) spa2-GFP:Kan^R ade6-M21X leu1-32 ura4-D18 h$^-$*	this study
KLG17855	*cdc15(E30K E152K) cdc12-mNeonGreen:Kan^R ade6-M21X leu1-32 ura4-D18 h$^-$*	this study
KLG17856	*cdc15(E30K E152K) pAct1-LifeAct-mCherry::leu1$^+$ ade6-M21X leu1-32 ura4-D18 h$^-$*	this study
KLG17857	*cdc15(E30K E152K) GFP-myo2:kan^R ade6-M21X leu1-32 ura4-D18 h$^-$*	this study
KLG17862	*cdc15(E30K E152K) bgs1-GFP:kan^R ade6-M21X leu1-32 ura4-D18 h$^-$*	this study
KLG17858	*cdc15(E30K E152K) GFP-bgs4::leu1$^+$ ade6-M21X leu1-32 ura4-D18 h$^-$*	this study
KLG16618	*cdc15(K163E):Kan^R ade6-M21X leu1-32 ura4-D18 h$^-$*	this study
KLG17397	*cdc15(K163E):Kan^R rgf3-GFP:Kan^R ade6-M21X leu1-32 ura4-D18 h$^-$*	this study
KLG17398	*cdc15(K163E):Kan^R fic1-GFP:Kan^R ade6-M21X leu1-32 ura4-D18 h$^-$*	this study
KLG17396	*cdc15(K163E):Kan^R pxl1-GFP:Kan^R ade6-M21X leu1-32 ura4-D18 h$^-$*	this study
KLG17399	*cdc15(K163E):Kan^R spa2-GFP:Kan^R ade6-M21X leu1-32 ura4-D18 h$^-$*	this study
KLG17507	*cdc15(K163E):Kan^R cdc12-mNeonGreen:Hyg^R ade6-M21X leu1-32 ura4-D18 h$^-$*	this study
KLG17516	*cdc15(K163E):Kan^R pAct1-LifeAct-mCherry::leu1$^+$ ade6-M216 leu1-32 ura4-D18 h$^-$*	this study
KLG17515	*cdc15(K163E):Kan^R GFP-myo2:Kan^R ade6-M21X leu1-32 ura4-D18 h$^-$*	this study
KLG17534	*cdc15(K163E):Kan^R bgs1-GFP:KanR leu1-32 ura4-D18 h$^-$*	this study
KLG17513	*cdc15(K163E):Kan^R GFP-bgs4::leu1$^+$ bgs4::ura4$^+$ leu1-32 ura4-D18*	this study
KLG17800	*cdc15(Core-4A):Kan^R ade6-M21X leu1-32 ura4-D18 h$^-$*	this study
KLG17803	*cdc15(Core-4A):Kan^R rgf3-GFP:Kan^R ade6-M21X leu1-32 ura4-D18 h$^-$*	this study
KLG17804	*cdc15(Core-4A):Kan^R fic1-GFP:Kan^R ade6-M21X leu1-32 ura4-D18 h$^-$*	this study
KLG17801	*cdc15(Core-4A):Kan^R pxl1-GFP:Kan^R ade6-M21X leu1-32 ura4-D18 h$^-$*	this study
KLG17802	*cdc15(Core-4A):Kan^R spa2-GFP:Kan^R ade6-M21X leu1-32 ura4-D18 h$^-$*	this study
KLG17886	*cdc15(Core-4A):Kan^R cdc12-mNeonGreen:Kan^R ade6-M21X leu1-32 ura4-D18 h$^-$*	this study
KLG17806	*cdc15(Core-4A):Kan^R pAct1-LifeAct-mCherry::leu1$^+$ ade6-M21X leu1-32 ura4-D18 h$^-$*	this study

KLG17849	*cdc15(Core-4A):Kan^R GFP-myo2:Kan^R ade6-M21X leu1-32 ura4-D18 h$^-$*	this study
KLG17887	*cdc15(Core-4A):Kan^R Bgs1-GFP:Kan^R ade6-M21X leu1-32 ura4-D18 h$^-$*	this study
KLG17805	*cdc15(Core-4A):Kan^R GFP-bgs4::leu1$^+$ ade6-M21X leu1-32 ura4-D18 h$^-$*	this study
KLG16014	*cdc15(K163A, R177A, R181A, K185A) ade6-M21X leu1-32 ura4-D18 h$^-$*	
KLG17818	*cdc15(E30K E152K)(1-849):KanR ade6-M21X leu1-32 ura4-D18 h$^-$*	this study
KLG17714	*cdc15(Core-4A) ade6-M21X leu1-32 ura4-D18 h$^-$*	this study
KLG17782	*cdc15(Core-4E) ade6-M21X leu1-32 ura4-D18 h$^-$*	this study
KLG17892	*cdc15(Core-4A Tip-4A) ade6-M21X leu1-32 ura4-D18 h$^-$*	this study
KLG10303	*cdc15(27A) ade6-M21X leu1-32 ura4-D18 h$^-$*	(Roberts-Galbraith et al., 2010)
KLG9723	*cdc15(27D) ade6-M21X leu1-32 ura4-D18 h$^-$*	(Roberts-Galbraith et al., 2010)
KLG18293	*cdc15(E30K, E152K, 27A) ade6-M21X leu1-32 ura4-D18 h$^-$*	this study
KLG18294	*cdc15(E30K, E152K, 27D) ade6-M21X leu1-32 ura4-D18 h$^-$*	this study
Figure S8		
KLG2971	*myo2-E1 ade6-M216 leu1-32 ura4-D18 h$^+$*	lab stock
KLG3354	*imp2::ura4$^+$ ade6-M210 leu1-32 ura4-D18 h$^+$*	lab stock
KLG441	*cdc4-8 ade6-M210 ura4-D18 h$^+$*	lab stock
KLG6614	*rng2-D5 ade6-M210 leu1-32 ura4-D18 h$^+$*	lab stock
KLG7144	*pxl1::ura4$^+$ ade6-M210 leu1-32 ura4-D18 h$^+$*	lab stock
KLG11730	*sid2-250 ade6-M210 leu1-32 ura4-D18 h$^+$*	lab stock
KLG1002	*cdc12-112 ade6-M212 leu1-32 ura4-D18 h$^+$*	lab stock
KLG2153	*cps1-191 ade6-M210 ura4-D18 lys1-131 h$^-$*	lab stock
KLG15485	*mid1::ura4$^+$ ade6-M21X leu1-32 ura4-D18 h$^-$*	lab stock
KLG3026	*clp1::ura4$^+$ ade6-M216 leu1-32 ura4-D18 h$^+$*	lab stock
KLG702	*cdc16-116 ade6-M210 leu1-32 ura4-D18 h$^+$*	lab stock
KLG12922	*rgf3-s44 his3-27 leu1-32 ura4-D18 h$^-$*	lab stock
KLG6008	*fic1::ura4$^+$ ade6-M21X leu1-32 ura4-D18 h$^+$*	lab stock
KLG8152	*spa2::ura4$^+$ ade6-M210 leu1-32 ura4-D18 h$^+$*	lab stock
KLG17819	*cdc15(E30K E152K):Hygr^R ade6-M21X leu1-32 ura4-D18 h$^-$*	this study
KLG17888	*cdc15(E30K E152K):Hygr^R cdc12-112 ade6-M21X leu1-32 ura4-D18 h$^-$*	this study
KLG17893	*cdc15(E30K E152K):Hygr^R cps1-191 ade6-M21X ura4-D18 lys1-131 h$^-$*	this study
KLG17890	*cdc15(E30K E152K):Hygr^R mid1::ura4$^+$ ade6-M21X leu1-32 ura4-D18 h$^-$*	this study
KLG17895	*cdc15(E30K E152K):Hygr^R clp1::ura4$^+$ ade6-M21X leu1-32 ura4-D18 h$^-$*	this study
KLG17896	*cdc15(E30K E152K):Hygr^R cdc16-116 ade6-M21X leu1-32 ura4-D18 h$^-$*	this study
KLG17897	*cdc15(E30K E152K):Hygr^R rgf3-s44 ade6-M21X leu1-32 ura4-D18 h$^-$*	this study

KLG17889	*cdc15(E30K E152K):Hygr^{R} fic1::ura4^{+} ade6-M21X leu1-32 ura4-D18 h^{-}*	this study
KLG17898	*cdc15(E30K E152K):Hygr^{R} spa2::ura4^{+} ade6-M21X leu1-32 ura4-D18 h^{-}*	this study

Supplemental References

Bähler, J., Wu, J., Longtine, M.S., Shah, N.G., McKenzie III, A., Steever, A.B., Wach, A., Philippsen, P., Pringle, J.R., 1998. Heterologous Modules for Efficient and Versatile PCR-based Gene Targeting in Schizosaccharomyces pombe. Yeast 14, 943–951.

Bai, X., Meng, G., Luo, M., Zheng, X., 2012. The rigidity of the wedge loop in PACSIN 3 is a key factor in dictating the diameters of tubules. J. Biol. Chem. 287, 22387–22396.

Carlson, B.R., Lloyd, K.E., Kruszewski, A., Kim, I.-H., Rodriguiz, R.M., Heindel, C., Faytell, M., Dudek, S.M., Wetsel, W.C., Soderling, S.H., 2011. WRP/srGAP3 facilitates the initiation of spine development by an inverse F-BAR domain, and its loss impairs long-term memory. J. Neurosci. 31, 2447–60.

Cortés, J.C.G., Carnero, E., Ishiguro, J., Sánchez, Y., Durán, A., Ribas, J.C., 2005. The novel fission yeast (1,3)beta-D-glucan synthase catalytic subunit Bgs4p is essential during both cytokinesis and polarized growth. J. Cell Sci. 118, 157–174.

Coutinho-Budd, J., Ghukasyan, V., Zylka, M.J., Polleux, F., 2012. The F-BAR domains from srGAP1, srGAP2 and srGAP3 regulate membrane deformation differently. J. Cell Sci. 125, 3390–401.

Guerrier, S., Coutinho-Budd, J., Sassa, T., Gresset, A., Jordan, N.V., Chen, K., Jin, W.-L., Frost, A., Polleux, F., 2009. The F-BAR domain of srGAP2 induces membrane protrusions required for neuronal migration and morphogenesis. Cell 138, 990–1004.

Henne, W., Boucrot, E., Meinecke, M., Evergren, E., Vallis, Y., Mittal, R., McMahon, H.T., 2010. FCHo proteins are nucleators of clathrin-mediated endocytosis. Science. 328, 1281–1284.

Huang, J., Huang, Y., Yu, H., Subramanian, D., Padmanabhan, A., Thadani, R., Tao, Y., Tang, X., Wedlich-Soldner, R., Balasubramanian, M.K., 2012. Nonmedially assembled F-actin cables incorporate into the actomyosin ring in fission yeast. J. Cell Biol. 199, 831–847.

Kakimoto, T., Katoh, H., Negishi, M., 2006. Regulation of neuronal morphology by Toca-1, an F-BAR/EFC protein that induces plasma membrane invagination. J. Biol. Chem. 281, 29042–53.

Keeney, J.B., Boeke, J.D., 1994. Efficient Targeted Integration at leu1-32 and ura4-294 in Schizosaccharomyces pombe. Genetics 136, 849–856.

Shimada, A., Takano, K., Shirouzu, M., Hanawa-Suetsugu, K., Terada, T., Toyooka, K., Umehara, T., Yamamoto, M., Yokoyama, S., Suetsugu, S., 2010. Mapping of the basic amino-acid residues responsible for tubulation and cellular protrusion by the EFC/F-BAR domain of pacsin2/Syndapin II. FEBS Lett. 584, 1111–8.